

Constrained Optimization Multi-dimensional Harmonic Balance Method for Quasi-periodic Motions of Nonlinear Systems

Haitao Liao¹

Abstract: The constrained optimization multi-dimensional harmonic balance method for calculating the quasi-periodic solutions of nonlinear systems is presented. The problem of determining the worst quasi-periodic response is transformed into a nonlinear optimization problem with nonlinear equality constraints. The general nonlinear equality constraints are built using a set of nonlinear algebraic equations which is derived using the multi-dimensional harmonic balance method. The Multi-Start algorithm is adopted to solve the resulting constrained maximization problem. Finally, the validity of the proposed method is demonstrated with a Duffing oscillator and numerical case studies for problems with uncertainties are performed on a nonlinear two-degree of freedom with non-regular nonlinearities. It is illustrated that the proposed approach can be used to find the worst resonant response and the upper and lower response bounds of quasi-periodic solution and is also able to quantify the combined influences of structural uncertainties and non-regular nonlinearities on the nonlinear quasi-periodic vibrations of nonlinear systems.

Keywords: Quasi-Periodic solution, multi-dimensional harmonic balance method, the MultiStart Algorithm, uncertainty.

1 Introduction

The method of determining periodic solutions of nonlinear systems is one of the most important fields in nonlinear dynamics researches. Many approaches have been developed to approximate periodic solutions of nonlinear systems. The harmonic balance method (HBM) is a well-known method to obtain approximate periodic solutions of nonlinear differential equations by using a truncated Fourier series. Many variants on the HBM have emerged. For example, Lau and Cheung (1981) proposed the incremental harmonic balance method. Cameron and Griffin (1989) pioneered the development of the alternating frequency/time domain (AFT)

¹ Chinese Aeronautical Establishment, Beijing 100012, China. Email: ht0819@163.com

method. Based on augmented Lagrangian to deal with nonsmooth contact-friction laws, Nacivet, Pierre and Thouverez (2003) proposed the dynamic Lagrangian frequency - time (DLFT) method. This method has been successfully used to quantify the efficiency of friction ring dampers [Laxalde, Thouverez, and Sinou (2007)]. Hall, Thomas, and Clark (2002) developed an improved version of the HBM which is referred to as the high dimensional harmonic balance (HDHB) approach in this study. The HDHB method was successfully improved to investigate the aeroelastic motions of an airfoil [Liu, Dowell, and Thomas (2007)]. In the HDBD method, aliasing [Liu, Thomas, and Dowell (2006)] can occur because higher harmonics will be introduced due to the nonlinear term. LaBryer described this phenomenon [LaBryer and Attar (2009)] and proposed filters to decrease aliasing. Cochelin et al. and Vergez (2009) presented another strategy for applying the classical HBM with a large number of harmonics. The basic idea consists in recasting the original system into a new system where nonlinearities are at most quadratic polynomials by introducing as many new variables as needed. Recently, a constrained harmonic balance method [Sarrouy, Dessombz, and Sinou (2013)] which computes solutions for periodic autonomous systems has been proposed. In the constrained harmonic balance method, a square system of nonlinear equations is generated by setting an unknown variable to a given value so that the size of the nonlinear algebraic equations is as many as unknowns. In order to estimate the number of selected harmonics for a given level of accuracy and reduce the size of the set of nonlinear algebraic equations, an adaptive harmonic balance method was developed by Jaumouillé, Sinou, and Petitjean (2010). A global analysis method [Sarrouy and Thouverez (2010)] mixing a harmonic balance method and a homotopy technique is presented to find all the periodic solutions of a nonlinear system. More recently, Dai, Schnoor, and Atluri (2012); Dai, Yue, and Yuan (2013) proposed a time domain collocation method and revealed its equivalence with the high dimensional harmonic balance method. The HDHB method has been proved to be a cumbersome version collocation method in disguise.

By making use of the harmonic balance method, a set of nonlinear algebraic equations is formed and is therefore well-determined. A nonlinear solver is then used to find zeros of such nonlinear equations. However, in order to perform parametric studies the nonlinear solver must be applied recursively.

In most industrial problems, the highest forced response levels are of major interests because of their defining effect on high cycle fatigue failures. The resonance response levels and resonance frequencies are dependent on design parameters of a nonlinear structure and on excitation levels. Moreover, in design practice there is usually a need to understand how design parameters affect the worst resonance response level and therefore forced response calculation has to be repeated over a

frequency range of interest for different parameter sets. Such parametric studies of the forced response can require large computational expense. Because of this, there is a need in the development of methods facilitating parametric analysis of nonlinear structures. Furthermore, the location of the nonlinear resonance extremum is a difficult problem [see Alexander (2010)]. Therefore, there is a need to locate the nonlinear resonance extremum and the nonlinear resonant frequency.

As mentioned previously, the harmonic balance method is limited to find periodic solutions (i.e a single fundamental frequency) and is unfit when the main frequencies of the system are not integers multiple of each other. The single-frequency harmonic balance method is therefore extended to the case where the solution is not periodic in time but is quasi-periodic. The first formal presentation of the harmonic balance method to obtain the quasi-periodic solutions of nonlinear systems is usually credited to Chua and Ushida (1981). Following the pioneer work of Chua and Ushida (1981) in electronics, a similar approach named the incremental harmonic balance method with multiple time scales was reported by Lau and Cheung (1983) and it was further developed by Pušenjāk and Oblak (2004) to handle general multi-degree of freedom externally excited and autonomous dynamical systems with cubic nonlinearities. By utilizing the AFT method in conjunction with multi-frequency Fourier transforms, the multi-dimensional harmonic balance method (MHBM) [Kim and Noah (1996); Kim and Choi (1997)] was proposed to study the internal resonant vibrations of a nonlinear Jeffcott rotor with contact terms. The multi-dimensional harmonic balance method with arc-length continuation was extended to the nonlinear vibration analysis of a modified Jeffcott rotor with piece-wise radial stiffness [Guskov, Sinou and Thouverez (2008)]. Based on the approximation of the frequency basis by a mono-dimensional one, a new methodology called the adjusted harmonic balance method [Guskov and Thouverez (2012)] has been introduced.

Most structural and mechanical systems are subject to variability and uncertainty in real life. Thus, the performance characteristics of such systems are also subject to uncertainties. In structural dynamics, taking into account uncertainty is important for various reasons: to increase the robustness of design, to ensure the compliance of vibration levels to standards, to assess worst case behavior and so on. In many instances, simulating solutions using a deterministic model may lead to inaccurate computational results. Therefore, any realistic analysis of nonlinear systems must take the uncertainties into account. The uncertainty analysis of nonlinear systems has received considerable attention. The Monte Carlo simulation (MCS) is a standard technique which has been widely used in engineering community for stochastic simulations. However, MCS requires a tremendous computational cost.

There is a growing interest to develop efficient computational algorithms for un-

certainty investigations in nonlinear systems. Different computational methodologies have been developed to quantify the uncertain response of nonlinear systems subject to parametric variability. The uncertainty in nonlinear systems can be modeled using probabilistic, interval or other methods. When the uncertain parameters are described as random variables with known probability distributions, the probabilistic methods can be used. In recent years, Polynomial Chaos Expansion (PCE), which helps to describe random functions with convergent polynomial functions series in some independent random variables with joint density functions, has been applied to many engineering problems taking into account the effects due to uncertainty. The polynomial chaos expansion combining with the harmonic balance method [Sinou and Faverjon (2012); Didier, Sinou, and Faverjon (2012)] is presented and applied to predict the dynamic behaviors in uncertain rotor systems with faults or cracks. By incorporating the polynomial chaos expansion with the multi-dimensional harmonic balance method, Didier, Sinou, and Faverjon (2013) developed the Stochastic multi-dimensional harmonic balance method. Unfortunately, the probabilistic approaches require a wealth of data, often unavailable, to define the probability density function of the uncertain structural parameters. Furthermore, Millman, King, and Beran (2005) found that the polynomial chaos expansion fail to predict limit cycle oscillations.

In many real situations, the maximum possible ranges of variations expressed in terms of percentage of the corresponding nominal of the parameters are only known and can be modeled as uncertain but bounded type parameters. In such cases, the interval analysis method [Moens and Vandepitte (2005)] is a viable alternative. However, the interval analysis often leads to an overestimation of the interval width [Wu, Zhang, and Chen (2013)]. Hence, reducing the overestimation in the interval method is a crucial issue to a successful interval analysis. To overcome these limitations, the objective of the present work is to develop a systematic methodology to determine the quasi-periodic solutions of nonlinear systems in the presence of uncertainty.

Remainder of this paper is organized as follows: the general formulation of the proposed method for determining the quasi-periodic solutions is presented in section 2. Validations of the proposed method are then conducted in section 3, which gives some numerical examples. Finally, concluding remarks are presented and discussed in Section 4.

2 The proposed method

A method named constrained optimization multi-dimensional harmonic balance method (COMHBM) which combines the multi-dimensional harmonic balance method and the MultiStart optimization algorithm is proposed in this section. The proposed

method is formulated as a constrained, nonlinear optimization problem. This paper is devoted to study the worst resonant quasi-periodic response in nonlinear structure. Therefore, the maximum vibration response expressed by the norm of the Fourier coefficient can be set as the optimization objective of the nonlinear optimization problem.

Within the framework of nonlinear constraints optimization theory, the nonlinear algebraic equations derived from the multi-dimensional harmonic balance method are treated as the generally nonlinear equality constraints. With the nonlinear equality constraints, the MultiStart algorithm is selected to find the worst resonant quasi-periodic response of nonlinear systems. The proposed method is the first to consider the multi-dimensional harmonic balance nonlinear algebraic equations as the nonlinear equality constraints of the nonlinear constrained optimization problem.

2.1 The nonlinear equality constraints derived from the multi-dimensional harmonic balance method

To obtain the quasi-periodic solutions of nonlinear systems, the multi-dimensional harmonic balance method is adopted. To present the method, the following equation of motion with n degree of freedom is considered:

$$M\ddot{\mathbf{u}} + D\dot{\mathbf{u}} + K\mathbf{u} + \mathbf{f}_{nl}(\mathbf{u}, \dot{\mathbf{u}}, t) = \mathbf{p}(t) \tag{1}$$

where M, C and K denote the mass, damping, and stiffness matrices, $\mathbf{p}(t)$ stands for the time dependent external force, \mathbf{u} , $\dot{\mathbf{u}}$, and $\ddot{\mathbf{u}}$ are respectively the displacement, velocity, acceleration vectors, and $\mathbf{f}_{nl}(\mathbf{u}, \dot{\mathbf{u}}, t)$ means the nonlinear force.

In the multi-dimensional harmonic balance method, the unknown time function $\mathbf{x}(t)$ can be written as a multiple Fourier series:

$$\mathbf{u}(t) = \sum_{k \in Z^M} [U_k^c \cos(k, \boldsymbol{\omega})t + U_k^s \sin(k, \boldsymbol{\omega})t] \tag{2}$$

where U_k^c and U_k^s are the Fourier coefficients vectors. The vector $\boldsymbol{\omega} = [\omega_1, \omega_2, \dots, \omega_M]$ is the incommensurable frequencies basis. $k = [k_1, \dots, k_M]$ with $k_j = -N, -N+1, \dots, -1, 0, 1, \dots, N+1, N$ where N is the order of the Fourier series stands for the harmonic index combination vector and (\cdot) represents the dot product

$$(k, \boldsymbol{\omega})t = \sum_{i=1}^M k_i \omega_i t \tag{3}$$

In the present work, the following condition for retaining N harmonics is adopted[18]:

$$\sum_{i=1}^M |k_i| \leq N \tag{4}$$

which leads to the presence of N_H harmonic terms $N_H = \frac{(2N+1)^M+1}{2}$.

With the use of Eq.(4), substituting Eq.(2) into Eq.(1) and equating the coefficients of the harmonic terms yield the following nonlinear function:

$$\mathbf{g}(\mathbf{U}, \omega) = \mathbf{A}(\omega)\mathbf{U} - \mathbf{b}(\mathbf{U}, \omega) = 0 \tag{5}$$

where $\mathbf{b} = \left[(\mathbf{C}_0)^T (\mathbf{C}_{k_1}^c)^T (\mathbf{S}_{k_1}^s)^T \dots (\mathbf{C}_{k_j}^c)^T (\mathbf{S}_{k_j}^s)^T \dots (\mathbf{C}_{k_{N_H}}^c)^T (\mathbf{S}_{k_{N_H}}^s)^T \right]^T$ corresponds to the Fourier coefficients of the nonlinear forcing term and the external force; $\mathbf{A}(\omega)$ and \mathbf{U} are respectively defined by

$$\mathbf{A} = \text{diag} \left(\mathbf{K}, \begin{bmatrix} \mathbf{K} - (\mathbf{k}_1, \omega)^2 \mathbf{M} & (\mathbf{k}_1, \omega) \mathbf{D} \\ -(\mathbf{k}_1, \omega) \mathbf{D} & \mathbf{K} - (\mathbf{k}_1, \omega)^2 \mathbf{M} \end{bmatrix}, \dots, \begin{bmatrix} \mathbf{K} - (\mathbf{k}_j, \omega)^2 \mathbf{M} & (\mathbf{k}_j, \omega) \mathbf{D} \\ -(\mathbf{k}_j, \omega) \mathbf{D} & \mathbf{K} - (\mathbf{k}_j, \omega)^2 \mathbf{M} \end{bmatrix}, \dots, \begin{bmatrix} \mathbf{K} - (\mathbf{k}_{N_H}, \omega)^2 \mathbf{M} & (\mathbf{k}_{N_H}, \omega) \mathbf{D} \\ -(\mathbf{k}_{N_H}, \omega) \mathbf{D} & \mathbf{K} - (\mathbf{k}_{N_H}, \omega)^2 \mathbf{M} \end{bmatrix} \right)$$

$$\mathbf{U} = \left[(\mathbf{U}_0)^T (\mathbf{U}_{k_1}^c)^T (\mathbf{U}_{k_1}^s)^T \dots (\mathbf{U}_{k_j}^c)^T (\mathbf{U}_{k_j}^s)^T \dots (\mathbf{U}_{k_{N_H}}^c)^T (\mathbf{U}_{k_{N_H}}^s)^T \right]^T \tag{6}$$

The difficulty with solving Eq.(5) is in finding a relationship between $\mathbf{b}(\mathbf{U}, \omega)$ and \mathbf{U} since the Fourier coefficients of the nonlinear forcing term are implicit functions of the Fourier coefficients of the displacement. To overcome this difficulty, the alternating frequency time technique[2] shown in Eq.(7).is employed.

$$\mathbf{U} \xrightarrow{\text{IFFT}^n} \mathbf{u}(t) \Rightarrow \mathbf{f}_{nl}(\mathbf{u}, \dot{\mathbf{u}}, t) \xrightarrow{\text{FFT}^n} \mathbf{b}(\mathbf{U}, \omega) \tag{7}$$

The key idea of the multi-dimensional harmonic balance method is to find the unknown harmonic coefficients \mathbf{U} in Eq.(5). As the conventional MHBM is used, Eq.(5) is a set of nonlinear equations being directly solved by a Newton-Raphson-type procedure. However, when the response of the nonlinear structure is desired over a range of frequencies, the solution of Eq.(5) must be repeated at each frequency. Furthermore, the application of the Newton-Raphson-type method requires that the number of unknown variables is equal to the number of nonlinear equations, that is, Eq.(5) is a well-defined nonlinear system. However, if the nonlinear system of algebraic equations is under-defined, which the number of the unknown variables is greater than the number of nonlinear equations in Eq.(5), the root finding algorithm can't be used to determine the unknown harmonic coefficients. Fortunately, quasi-periodic solution can be obtained in another way once the nonlinear function of Eq.(5) is satisfied. Therefore, unlike the traditional implementations of the multi-dimensional harmonic balance method, the nonlinear function of Eq.(5) is used to construct the nonlinear equality constraints of optimization problem.

2.2 Optimization with GlobalSearch

As our objective of optimization is to find the optimal solution aiming to maximize the vibration response of the nonlinear system of Eq.(1), thus the nonlinear equality constraints of Eq.(5) have to be satisfied. Therefore, the following nonlinear optimization problem can be formulated:

$$\begin{aligned} f(\mathbf{x}) &= f(\mathbf{U}, \omega, \mathbf{v}_u) = \max \|\mathbf{U}\|_2 \\ \text{s.t } \mathbf{g}(\mathbf{x}) &= \mathbf{g}(\mathbf{U}, \omega, \mathbf{v}_u) = \mathbf{A}(\omega, \mathbf{v}_u)\mathbf{U} - \mathbf{b}(\mathbf{U}, \omega, \mathbf{v}_u) = 0 \end{aligned} \quad (8)$$

where $\mathbf{x} = \{\mathbf{U}, \omega, \mathbf{v}_u\}^T$, the symbol $\|\cdot\|$ denotes a vector norm and \mathbf{v}_u is a set of design parameters and/or uncertainty parameters.

The solution of this nonlinear optimization problem with respect to a vector of unknowns $\mathbf{x} = \{\mathbf{U}, \omega, \mathbf{v}_u\}^T$ gives a vector of Fourier coefficients \mathbf{U}^{opt} and a resonance frequency, ω^{opt} at a set of parameter values \mathbf{v}_u^{opt} . Their accurate and effective calculation is a very important problem, which is discussed in the following section.

The choice of optimization algorithm is very important, because the final results are usually dependent on the specific algorithm in terms of accuracy and local minima sensitivity. In this investigation, the advanced OptQuest NonLinear Programs (OQNLP) MultiStart gradient-based algorithm [Ugray, Lasdon and Plummer (2007)] along with the sequential quadratic programming(SQP) method[Nocedal and Wright (2006); Fletcher (2013)] as the local solver is implemented and the gradients are approximated by finite differences.

A flowchart of the OQNLP MultiStart algorithm is shown in Fig.1 in which SP(xt) stands for the starting point generator and xt represents the candidate starting point produced. Starting from the point xs , the local NLP solver L($xs; xf$) produces the final point xf . The function UPDATE LOCALS($xs; xf;w$) is then used to process and store solver output xf and the updated penalty weights, w is also calculated.

There are two stages of the algorithm. The algorithm performs n_1, n_2 iterations for the stage1 and stage2, respectively. At each iteration, the starting point generator SP(xt) produces the candidate starting point xt and this point is also used to calculate the L1 exact penalty value $P(xt,w) = f(xt) + \sum_{i=1}^{(2N_H+1)n} w_i \cdot viol(g_i(xt))$ where

w_i is the positive penalty weight and the function $viol(g_i(xt))$ equals the absolute violation of the i th equality constraint of problem Eq.(8) at point xt . After finishing n_1 iterations of stage 1, the local solver L is called at the best point that has the smallest value of P in stage 1. In stage 2, the MultiStart algorithm runs the local solver L starting at the points that pass the distance and merit filters. For the distance filter, the distance factor distfactor is used to determine whether a point is in an existing basin of attraction. For the merit filter, the threshold factor threshfactor

```

Stage 1
Call  $L(x0, xf)$  ( $x0$  = user initial point)
Call UPDATE LOCALS( $x0, xf, w$ )
For  $i = 1: n1$  Do
    Call SP( $xt(i)$ )
    Evaluate  $P(xt(i), w)$ 
EndDo
 $xt^*$  = point yielding best value of  $P(xt(i), w)$  over all stage one points ( $i = 1, 2, \dots, n1$ ).
call  $L(xt^*, xf)$ 
Call UPDATE LOCALS( $xt^*, xf, w$ )
threshold =  $P(xt^*, w)$ 
Stage 2
For  $i = 1: n2$  Do
    Call SP( $xt(i)$ )
    Evaluate  $P(xt(i), w)$ 
    Perform merit and distance filter tests:
    Call distance filter( $xt(i), dstatus$ )
    Call merit filter( $xt(i), threshold, mstatus$ )
    If ( $dstatus$  and  $mstatus = "accept"$ ) Then
        Call  $L(xt(i), xf)$ 
        Call UPDATE LOCALS( $xt(i), xf, w$ )
    EndIf
EndDo

```

Figure 1: A flowchart of the OQNLP MultiStart algorithm

and waitcycle are used to update threshold. The basin radius of the distance filter and the threshold of the merit filter are updated during the optimization process. A basin radius decreases after waitcycle consecutive start points. These two filters help the MultiStart algorithm to run with a few points and with high success rate. If the local solver L runs starting from the point that passes the distance and merit filters, it can yield a positive exit flag, which indicates convergence. A detailed analysis of the algorithm can be found in Ugray, Lasdon, and Plummer (2007).

Optimization experiments for the selected nonlinear dynamical systems show that other optimization methods such as Generic Algorithm, Differential Evolution and Particle Swarm Optimization etc fail to find the actual solution of Eq.(8) and the SQP method seems to be the best nonlinear programming method for the con-

strained optimization problem Eq.(8). It outperforms every other nonlinear programming method in terms of efficiency, accuracy, and percentage of successful solutions, over a large number of test problems. As for the MultiStart algorithm, the MultiStart algorithm owes much of its efficiency to its merit and distance filters and these two filters help the MultiStart algorithm to run the SQP method with a few starting points and high success rate. Therefore, the use of the MultiStart algorithm along with the SQP method is very important for finding the optimization solution of Eq.(8).

3 Application to select nonlinear dynamical systems

In order to demonstrate the effectiveness of the proposed method, two numerical examples which have been taken from recent publications [Guskov and Thouverez (2012); Didier, Sinou, and Faverjon, (2013)] are considered.

3.1 Duffing oscillator

3.1.1 The model

A classical nonlinear Duffing oscillator which has been used extensively in the literature is used as the first example. The equation of motion for the Duffing oscillator is given by

$$\ddot{u} + 2\zeta\dot{u} + u + \gamma u^3 = f_1 \sin(\omega_1 t) + f_2 \sin(\omega_2 t) \quad (9)$$

where ζ , γ are the damping coefficient and the nonlinear stiffness coefficient, respectively, f_1 and f_2 mean the force amplitudes. ω_1 and ω_2 are the two incommensurate excitation frequencies.

To align with the computational study of Guskov and Thouverez (2012), the following structural parameters were chosen: $\zeta=0.1$, $\gamma=0.2$, $f_1 = f_2=5$, $\omega_1/\omega_2 = \sqrt{2}$. The complete frequency response function shown in Fig.2 was obtained over the entire frequency range $[0.1,8](\text{rad/s})$ using an Arc-length continuation scheme, similar to that used in Guskov and Thouverez (2012).

It can be seen from Fig.2 that with a hardening spring($\gamma > 0$) the response curve tends to bend to the right and the system reaches the top amplitude at resonant peak P_{max} of which the corresponding frequency is $\omega_1 = 2.44(\text{rad/s})$. Five quasi-periodic solutions of which the upper and lower response bounds are P_{upp} and P_{low} respectively coexist at the excitation frequency $\omega_1 = 2.95(\text{rad/s})$. In the following, two cases are investigated by utilizing the proposed method:

(1)Case 1: searching the resonant peak P_{max}

In order to obtain the resonant peak P_{max} , the norm of Fourier coefficients \mathbf{U} is maximized. As explained previously, the unknown variables that have to be determined

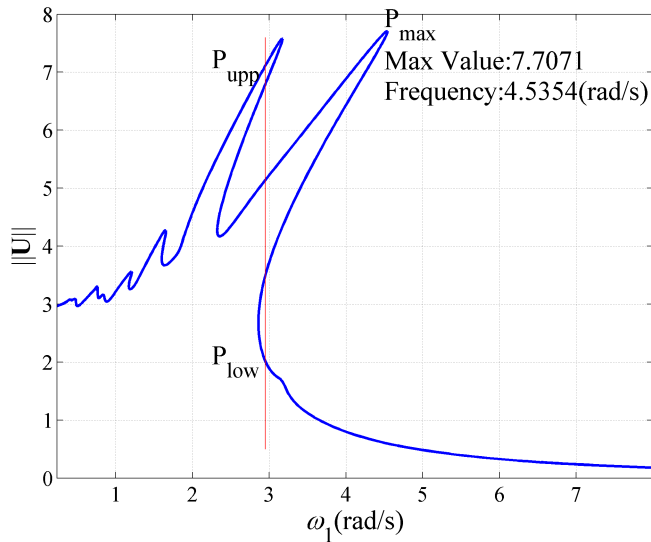


Figure 2: Frequency-response curve of the Duffing oscillator with multi-harmonic forcing

are the unknown Fourier coefficients \mathbf{U} and the frequency ω_1 of the quasi-periodic solution P_{low} .

(2)Case 2: finding the upper and lower response bounds at a given frequency

While looking for multiple solutions at a given frequency, the excitation frequency is not included as an optimization variable and the Fourier coefficients \mathbf{U} are the only unknown variables. It should be noted that the objective function in Eq.(8) is changed as the minimization of the norm $\|\mathbf{U}\|$ for searching the quasi-periodic solution .

3.1.2 Numerical results

(1)Optimization results by the proposed method

Based on the OQNLP MultiStart algorithm described in section 2.2, optimizations are then performed to find these quasi-periodic solutions and the parameters of the optimization algorithm are listed as follows: Number of trial points was chosen to be 1000, and the usual value of 200 for the number of Stage1 points has been taken. The maximum number of generations allowed for the SQP algorithm was 600 while the function tolerance and the nonlinear equality constraints tolerance were both set to 10⁻¹⁰. A frequency range from 0.1 to 8 (rad/s) was considered.

The number of harmonics retained N is 13 according to Guskov and Thouverez (2012);

After the MultiStart algorithm stops successfully, numerical results are obtained. The optimization results are reported in Fig.3 where the two dimensional time series are also plotted. The maximum values of the nonlinear equality constraints that were evaluated at these optimal solutions are $1.3301e-11$ for P_{max} , $4.2633e-13$ for P_{upp} and $7.2374e-11$ for P_{low} , which are less than the nonlinear equality constraints tolerance 10^{-10} . Therefore, the nonlinear algebraic equations in Eq.(5) are satisfied.

Observe in Fig.3 that the maximum resonance peak found by the proposed method is 7.7072 at the nonlinear resonance frequency 4.5349(rad/s). From Fig.2 one can easily find that the resonance response level has its maximum value 7.7071 at the resonance frequency 4.5354(rad/s). Comparison with Fig.2 shows that the proposed method really finds the resonance peak. In addition, it can be seen from Fig.3 that the presence of several harmonic components can be detected in the frequency spectrums and there is one main harmonic component in the system response. The solutions P_{max} and P_{low} are dominated by the harmonic component [0,1], whilst the solution P_{upp} is dominated by the harmonic component [1,0]. For P_{low} , the Duffing oscillator shows high magnitude oscillation not only at the harmonic component [0,1], rather it also exhibits harmonic response at the harmonic components [1,0],[1,2],[2,3]. It should be noted that for calculating the quasi-periodic solutions P_{upp} and P_{low} , the proposed method can be viewed as a root finding algorithm.

(2) Comparison with numerical integration results

In order to fully validate the proposed approach, direct numerical integrations have been performed. Numerical simulations are computed by the fourth order Runge–Kutta scheme with fixed step-size 0.001 here. The initial conditions can be readily supplied by the results of the presented method. In order to eliminate the transient part of the responses, the initial responses are discarded from the stored responses and results are plotted only for 900-1000. The time responses of the Duffing system at these optimal solutions using the time integration method and the proposed method are presented in Fig.4 where the absolute errors between the two methods are also shown for these optimal solutions. The solid line and dashed line denote the proposed method solutions and the numerical integration results respectively.

The results from the proposed method and from the time domain integration method are difficult to distinguish when they are plotted on the same graph. However, from the absolute errors in the time domain, the differences between numerical results from the proposed method and from the time integration method are clearly visible. Observe in Fig.4 that there are small errors in amplitude and the maximum

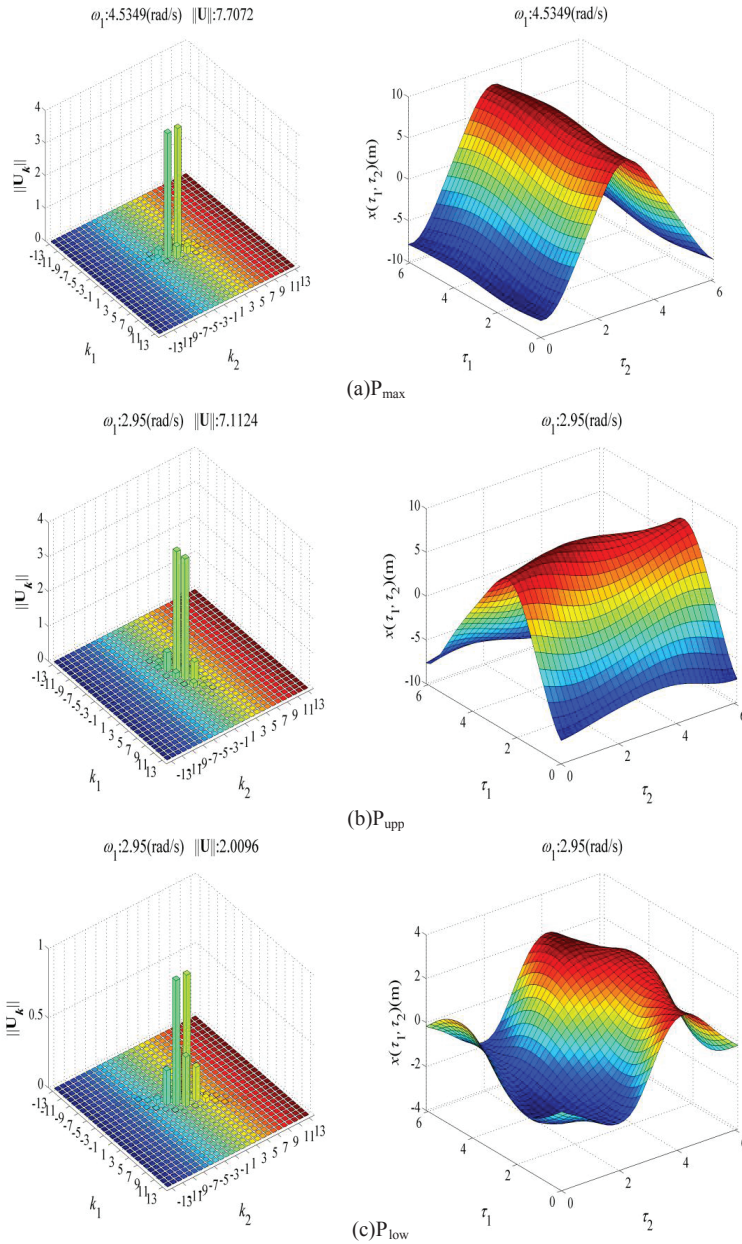


Figure 3: The optimization results obtained by the proposed method

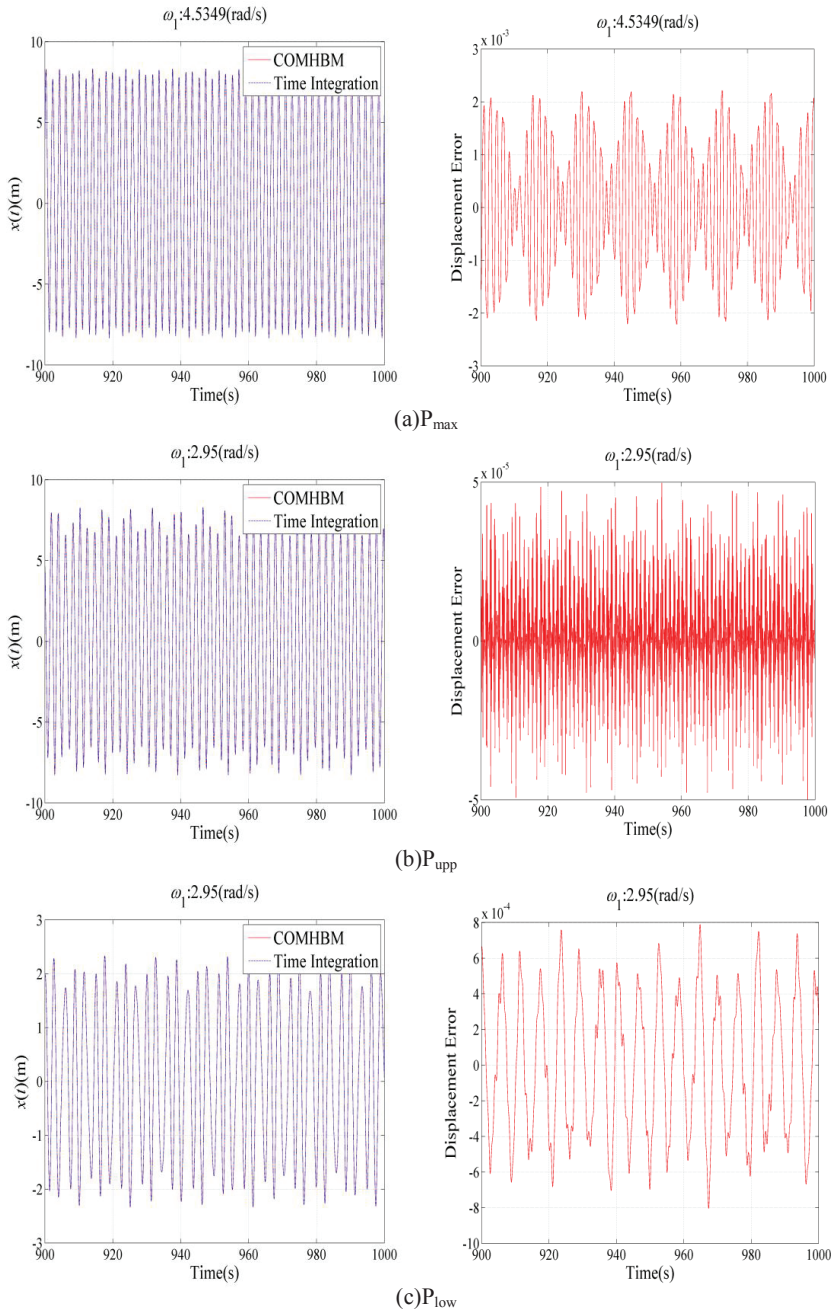


Figure 4: The time responses of the Duffing Oscillator

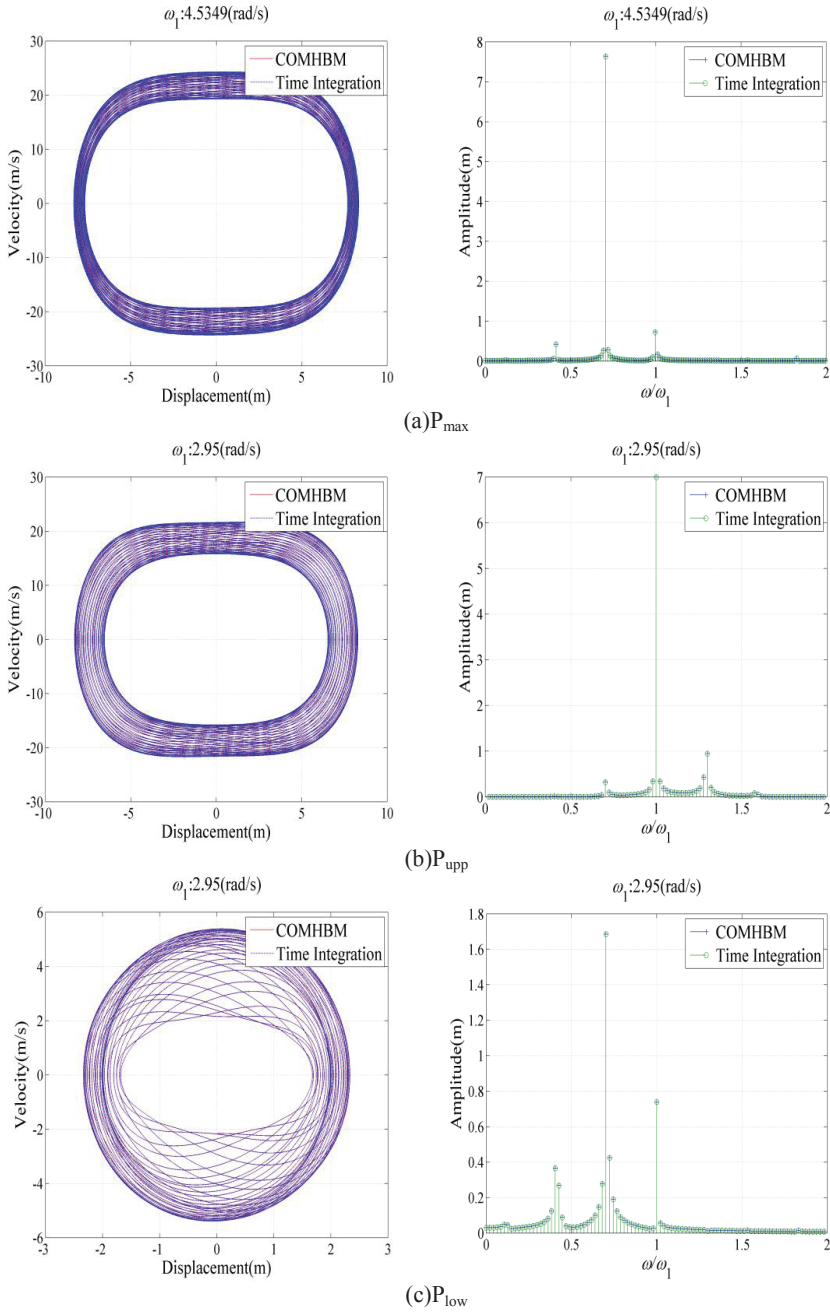


Figure 5: Phase portraits and its corresponding FFT of the quasi-periodic motions

error corresponds to the resonant peak P_{max} . For the resonant peak P_{max} in Fig.4, the maximum absolute difference between the responses as generated using the proposed method and the time integration method is less than $3e-3$ while the maximum absolute displacement errors for solutions P_{upp} and P_{low} are less than $5e-5$, $8e-4$ respectively. It is evident that the present approach solutions match well with the numerical integration solutions.

Fig.5 shows the phase portraits and the corresponding frequency spectrums at these three solutions. As shown in Fig. 5, many loops are seen in the phase plane portrait and phase plane portraits are banded attractors. The phase orbits and the associated spectrums, the shapes of which are close ring, all clearly indicate that the system is acting with quasi-periodic motions. For these solutions, there is one main harmonic terms in the system response and the presence of several harmonic components can be detected. For solution P_{max} , the frequency spectrum is primarily composed of ω_2 , the influence of other harmonic components being insignificant. The largest peak for solution P_{upp} is detected at a non-dimensional frequency 1 while for solution P_{low} , the system vibrates with the dominate frequency ω_2 and a number of smaller peaks is observed. It can be seen from Figs.4 and 5 that the proposed method is in excellent agreement with the time integration method both in time and frequency domains. The comparison between the proposed method and time integration method is extremely good.

The numerical simulations were performed on a Lenovo notebook computer with Intel Core processors i3-330M of 2.13GHz and 2GB DDR3 RAM. For finding solutions P_{max} , P_{upp} and P_{low} , the proposed method requires 625.7813, 587.5313, 466.9063 seconds to converge while the CPU time required by the continuation method to calculate the frequency response curve in Fig.2 is $3.7542e3$ seconds. It is obvious that the CPU time needed by the proposed method to obtain the worst-case forced response for a given frequency of the interval studied is much less than that of the multi-dimensional harmonic balance method along with the continuation method. The comparison of the computational cost shows the outstanding benefits that stem from the use of the present method.

3.2 A nonlinear two degree-of-freedom model with different types of nonlinearities and uncertainties

After the success of the proposed method in the above test model, the proposed method is applied to uncertainty quantification problems. The model considered by Didier, Sinou, and Faverjon (2013) is here chosen for the numerical simulations, as shown in Fig.6.

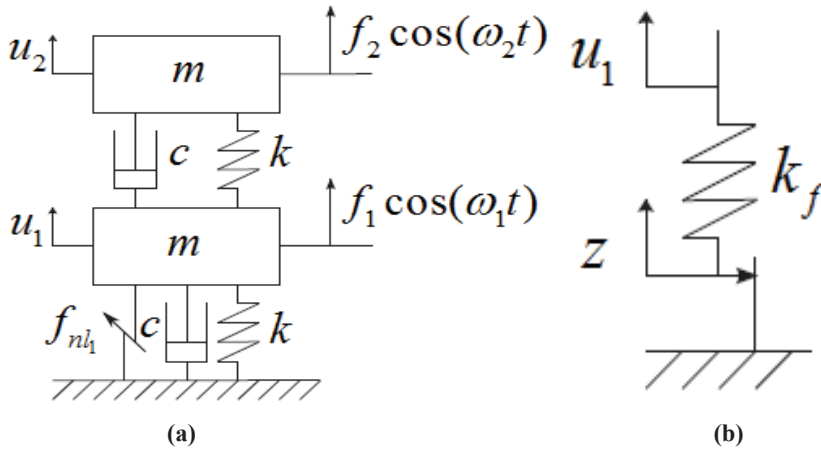


Figure 6: The nonlinear model

3.2.1 The nonlinear model

The system shown in Fig.6 was studied by Didier, Sinou, and Faverjon (2013) to evaluate the performance of the multi-dimensional harmonic balance method with the polynomial chaos expansion. Structural nonlinearity is applied only in the first degree of freedom. The governing dynamic equations of the problem can be expressed as follows:

$$\begin{bmatrix} m & 0 \\ 0 & m \end{bmatrix} \begin{pmatrix} \ddot{u}_1 \\ \ddot{u}_2 \end{pmatrix} + \begin{bmatrix} 2c & -c \\ -c & 2c \end{bmatrix} \begin{pmatrix} \dot{u}_1 \\ \dot{u}_2 \end{pmatrix} + \begin{bmatrix} 2k & -k \\ -k & 2k \end{bmatrix} \begin{pmatrix} u_1 \\ u_2 \end{pmatrix} + \begin{pmatrix} f_{nl_1}(t) \\ 0 \end{pmatrix} = \begin{pmatrix} f_1 \cos(\omega_1 t) \\ f_2 \sin(\omega_2 t) \end{pmatrix} \tag{10}$$

where m, c, k are respectively the mass ,damping coefficient and linear stiffness. $f_{nl_1}(t)$ means the nonlinear force. f_1 and f_2 denote the forcing amplitudes. ω_1 and ω_2 represent the two incommensurable excitation frequencies with $\omega_1/\omega_2 = \sqrt{2}$.

In the following, two kinds of nonlinear force are considered:

(1) Case 1: the contact force

The representation of the contact force is modeled as follows:

$$f_{nl_1}(t) = \begin{cases} k_1 u_1(t) & \text{if } |u_1(t)| \leq u_{lim} \\ k_2 u_1(t) - \text{sign}(u_1(t))(k_2 - k_1)u_{lim} & \text{if } |u_1(t)| > u_{lim} \end{cases} \tag{11}$$

where k_1 and k_2 define effective stiffness and u_{lim} represents the clearance value.

(2) Case 2: the friction force

The friction force $f_{nl_1}(t)$ shown in Fig.6(b) is represented as:

$$f_{nl_1}(t) = \begin{cases} k_f(u_1(t) - z(t)) & \text{if } |u_1(t)| \leq \mu P \\ \mu P \text{sign}(\dot{z}(t)) & \text{if } |u_1(t)| > \mu P \end{cases} \quad (12)$$

where k_f denotes the contact stiffness, μ stands for the friction coefficient, P is the normal pressure and $z(t)$ is the relative displacement of the contact point.

The deterministic system parameters for the model in Fig.6 are listed in Table 1 where \bar{k} and $\bar{\mu}$ are respectively the deterministic values of k and μ , which is borrowed from Didier, Sinou, and Faverjon (2013). The first-order and second-order natural frequencies of the underlying linear system are $fre_1=19.4924(\text{Hz})$ and $fre_2=33.7619(\text{Hz})$, respectively.

Table 1: Physical parameters of the system

Parameter	\bar{k}	m	c	f_1	f_2	k_1	k_2	k_f	$\bar{\mu}$	P
Value	15000	1	1	1	1	$5 \cdot 10^{-4}$	$5 \cdot 10^3$	3000	0.4	10
(Unit)	(N.m ⁻¹)	(kg)	(N.m ⁻¹ s ⁻¹)	(N)	(N)	(N.m ⁻¹)	(N.m ⁻¹)	(N.m ⁻¹)		(N)

3.2.2 Parameter uncertainties considered

In the following, the combined effects of parameter uncertainties and nonlinearities on the peak vibration response are investigated using the proposed method. Two cases of uncertainty with two external incommensurable frequencies ω_1 and ω_2 are considered. The excitation types applied to the model in Fig.6 are the same as case 6 and case 7 of Didier, Sinou and Faverjon (2013).

(1) Case1: uncertainty in the linear stiffness with the nonlinear contact force

A detuning parameter $v_u \in [0, 1]$ with the small parameter ξ_k is introduced to quantify the deviation of k from the linear stiffness \bar{k} , and $k(v_u)$ is described by

$$k = (1 - \xi_k + 2\xi_k * v_u)\bar{k} \quad (13)$$

with $\xi_k=0.05$.

(2) Case2: uncertainty in the friction coefficient

The parameter uncertainty is modeled as a variation in the friction coefficient as:

$$\mu = (1 - \xi_\mu + 2\xi_\mu * v_u)\bar{\mu} \quad (14)$$

with $\xi_\mu=0.025$. v_u varies from 0 to 1.

3.2.3 Numerical results

(1) Optimization results of the worst-case resonance response

Consider the optimization problem Eq.(8), the objective function to be optimized is the norm of the Fourier coefficients \mathbf{U} . Aiming at a maximization of the norm of the Fourier coefficients \mathbf{U} , the uncertainty variable v_u should be treated as optimization variable in the optimization problem of Eq.(8). Therefore, there are three categories of optimization variables including the uncertainty variable v_u , the unknown Fourier coefficients \mathbf{U} and the excitation frequency ω_1 . The approximation with one harmonic provides quite an accurate solution according to Didier, Sinou, and Faverjon (2013) and will be used in the rest of this paper. Optimizations are performed using the settings of the optimization algorithm similar to the first example. The optimization results for both cases are shown in Table 2 where also shows the worst resonance peaks of the deterministic systems. The nonlinear equality constraints that were evaluated at these optimization solutions are given in Table 2 where $\max(|\mathbf{g}(\mathbf{U}, \boldsymbol{\omega}, \mathbf{v}_u)|)$ stands for the maximum absolute error of the multi-dimensional harmonic balance equations Eq.(5).

Table 2: The optimization results obtained by the proposed method

		Case 1		Case 2	
		The deterministic system	The worst uncertain system	The deterministic system	The worst uncertain system
\mathbf{U}	$\mathbf{U}_{(0,0)}$	1.0308e-20	-6.7328e-20	-4.3801e-9	-4.3801e-9
		5.1539e-21	-3.3664e-20	-2.1900e-9	-2.1900e-9
	$U^c_{(0,1)}$	-3.8405e-3	-3.8679e-3	-4.0823e-3	-4.0823e-3
		-4.2953e-3	-4.3404e-3	-4.0827e-3	-4.0827e-3
	$U^s_{(0,1)}$	5.8192e-5	2.3939e-4	1.2017e-8	1.2000e-8
		9.4007e-5	2.9812e-4	3.3340e-5	3.3340e-5
$U^c_{(1,0)}$	1.3832e-5	1.4519e-5	-3.2851e-8	-3.2851e-8	
	-6.5705e-5	-6.7337e-5	-6.6632e-5	-6.6632e-5	
$U^s_{(1,0)}$	1.9757e-5	2.06343e-6	1.5384e-6	1.5384e-6	
	-1.0048e-6	-1.0478e-6	-4.6086e-7	-4.6086e-7	
ω_1		28.9857	28.6543	27.5660	27.5660
v_u			0		1
$\max(\mathbf{g}(\mathbf{U}, \boldsymbol{\omega}, \mathbf{v}_u))$		2.8422e-14	1.4864e-11	1.6395e-14	1.3548e-12
Objective Function Value		5.7633e-3	5.8266e-3	5.7740e-3	5.7740e-3

As can be seen from Table 2, for both cases the quasi-periodic responses are domi-

nated by the harmonic component $U_{(0,1)}^c$ and the nonlinear equality constraints are satisfied. For case 1, a maximum norm of $5.8266e-3$ was produced by the worst uncertain system at an excitation frequency of $28.6543(\text{Hz})$ while a maximum norm of $5.7633e-3$ was experienced by the deterministic system at an excitation frequency of $28.9857(\text{Hz})$. It is observed that the resonance frequency corresponding to the worst uncertain system is lower than that of the deterministic system and the norm $\|U\|$ for case 1 changes a little at most when v_u varies. The response for case 1 is at its maximum when $v_u=0$. Comparison the worst resonance responses between the deterministic system and the worst uncertain system for case 1 lead to the conclusion that a lower linear stiff k leads to a larger vibration response.

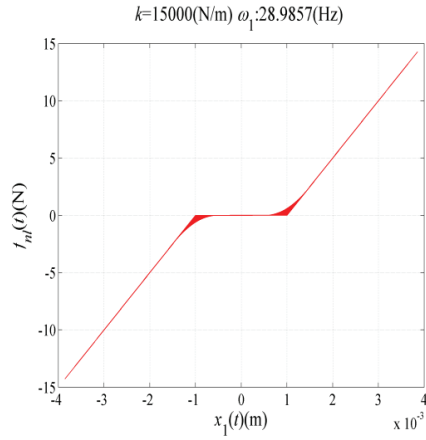
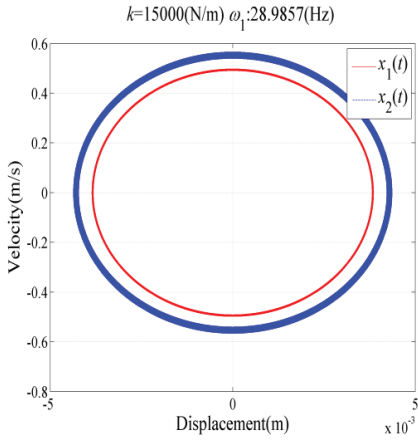
On the contrary, for case 2 the optimization results of the worst uncertain system are very much identical with that of the deterministic system and the value of the resonant peak and the resonant frequency do not change. The uncertainty of the friction coefficient does not affect the norm of the Fourier coefficients U . The worst resonance frequencies of the associated bi-periodic excitation are 27.5660 , which is equal to $\sqrt{2}\omega_1$.

The phase portraits and the nonlinear forces associated with these optimization solutions are illustrated in Fig.7. As illustrated in Fig.7, the phase plots for both cases are symmetric with respect to the coordinate line and the motions in phase space are ellipse. For case 1, the vibration responses of u_1 are lower than that of u_2 whilst for case 2 the trajectories on the phase plane for u_1 and u_2 are coincide with each other. In addition, classical hysteresis curves of the nonlinear force-displacement relationship can be observed in Fig.7(c) and Fig.7(d).

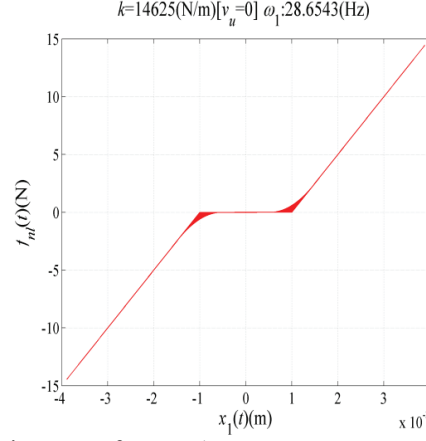
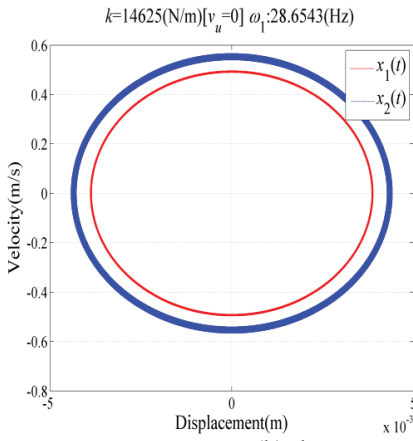
(2) Optimization results of the worst resonance response near the first natural frequency

In order to study the nonlinear dynamics near the first natural frequency, the proposed method is again employed to predict the worst resonance responses. The variable v_u describing the uncertainty is the decision variable of the optimization problem. The excitation frequency variable is limited to the frequency range $[18,22](\text{Hz})$. All other parameters are the same as in the previous studies. The optimization results obtained by the presented method are illustrated in Table 3.

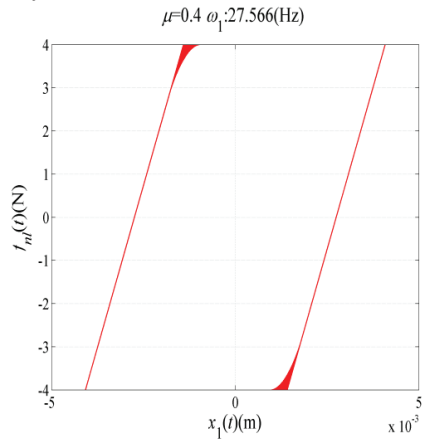
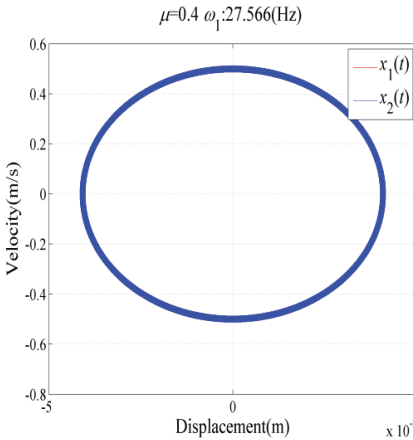
As shown in Table 3, it can be seen that the harmonic component $U_{(1,0)}^s$ dominates the quasi-periodic responses and the calculated worst resonance responses for both cases are slightly larger than the counterparts of the deterministic system. For case 1, a similar behavior has been found compared with the results in Table 1. For case 2, a maximum norm $2.2355e-3$ of the deterministic system is observed at a frequency of $20.3503(\text{Hz})$. On the other hand, the worst uncertain system has a peak response norm of $2.3253e-3$ at an excitation frequency of $20.3558(\text{Hz})$. The



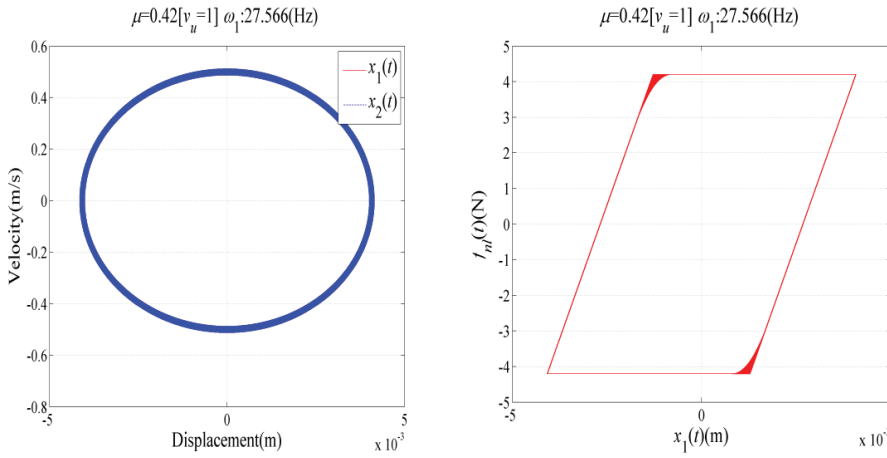
(a)The deterministic system for case 1



(b)The worst uncertain system for case 1



(c)The deterministic system for case 2



(d)The worst uncertain system for case 2

Figure 7: The worst time series and the nonlinear forces of the nonlinear models

Table 3: The optimization results obtained by the proposed method

		Case 1		Case 2	
		The deterministic system	The worst uncertain system	The deterministic system	The worst uncertain system
U	$\mathbf{U}_{(0,0)}$	2.5344e-21	-4.1020e-21	-1.1588e-20	-4.9528e-21
		1.2672e-21	-2.0545e-21	-5.7938e-21	-2.4764e-21
	$U_{(0,1)}^c$	-5.1437e-7	-5.3150e-7	-8.7024e-7	-8.7173e-7
		-8.0961e-7	-8.4086e-7	-1.0702e-6	-1.0718e-6
	$U_{(0,1)}^s$	4.4598e-5	4.5572e-5	5.9667e-5	5.9713e-5
		7.6740e-5	7.8667e-5	8.6821e-5	8.6870e-5
	$U_{(1,0)}^c$	1.1882e-4	1.1331e-4	-3.7701e-5	-3.8358e-5
		9.1777e-5	8.4793e-5	-5.8271e-5	-5.9730e-5
	$U_{(1,0)}^s$	3.4599e-3	3.4873e-3	1.5026e-3	1.5625e-3
		3.8465e-3	3.8893e-3	1.6504e-3	1.7173e-3
ω_1		20.4472	20.2163	20.3503	20.3558
v_u			0		1
$\max(\mathbf{g}(\mathbf{U}, \boldsymbol{\omega}, \mathbf{v}_u))$		4.1545e-13	9.3234e-11	9.7367e-13	2.2138e-12
Objective Function Value		5.1765e-3	5.2266e-3	2.2355e-3	2.3253e-3

resonance frequency corresponding to the worst uncertain system is higher than that of the deterministic system. Comparing the results between Table 2 and 3, it can be noted that for case 2 the nonlinearity only affects the dynamics of the resonance peak near the first natural frequency fre_1 whereas the dynamics of the worst resonance peak are not affected by the nonlinearity. In addition, it is interesting that the uncertainty values v_u for case 1 and 2 are anomalously different. The vibration response for case 1 reaches the resonance peak of $5.2266e-3$ when the coefficient of linear stiffness approaches its lower bound while the norm $\|U\|$ for case 2 takes its maximum when $v_u = 1$.

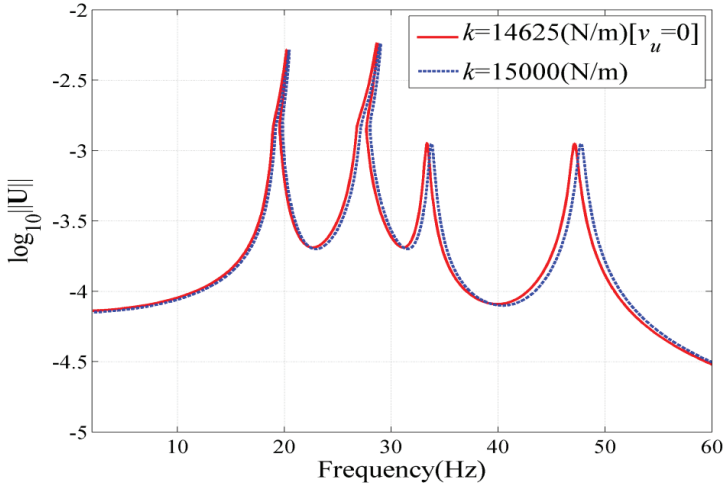
(3) The frequency response curves of the worst uncertain systems

For comparison, forced responses of the worst resonant scenarios listed in Table 2 and 3 are also calculated as a function of excitation frequency using the multi-dimensional harmonic balance method with the continuation method. Frequency response curves are drawn in Fig.8 for case 1 and Fig.9 for case 2. In Fig.8 and Fig.9, a zoom on the first two resonance peaks is done.

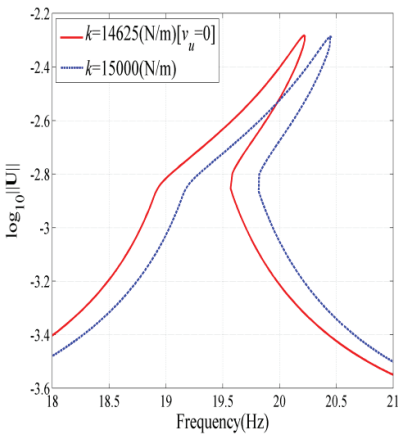
As can be seen in Fig.8 and Fig.9, four main resonance peaks are observed and the peaks of the frequency response curves are sharp and narrow. As expected, the first two most important peaks are near the first natural frequency fre_1 of the underlying linear system. The response curves for case 1 show hardening-spring nonlinear characteristics and the resonant peaks of the worst uncertain system shift towards left slightly. The softening behavior of the system is confirmed in Fig.9. It is noted that for case 1 the resonant peaks of the worst uncertain system are slightly higher than the counterparts of the determined system while for case 2 the friction coefficient has no effect on the largest resonant peak. However, in the vicinity of the first resonant peak for case 2, discrepancy is observed but remains very small. Therefore, the results in Table 2 and 3 are validated by comparison with the conventional calculation of the forced response curves in Fig.8 and Fig.9.

(4) Comparison with Monte Carlo simulation results

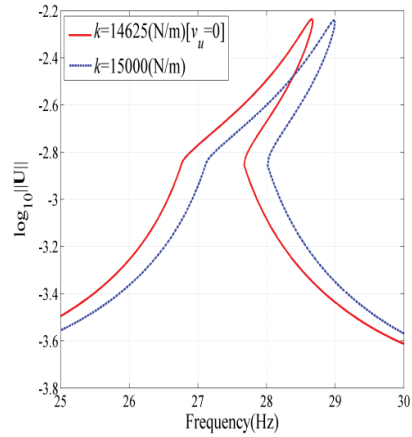
The last part of this section is dedicated to the efficiency of the proposed method compared to Monte Carlo simulation. In Monte Carlo simulation, a series of quasi-periodic solutions can be obtained by taking all values over the considered bounded regions of v_u . With the aid of the attained solutions, the bounds and some properties of the quasi-periodic motions are determined and compared with the results in Table 2 and 3. Fig.10 shows the influences of the linear stiffness k and the friction coefficient μ on the norm of U . The curves shown in Fig.10 are obtained by taking the norm $\|U\|$ for all realizations at each v_u . For case 1, the norm $\|U\|$ for the first two resonant peaks varies very slowly with respect to v_u and it decreases monotonically when v_u increases from 0 to 1. Therefore, the norms of the previous



(a)The overall frequency response curves



(b)Zoom-in part showing the first resonance peaks



(c)Zoom-in part showing the second resonance peaks

Figure 8: The frequency response curves for case 1

two peaks are monotonically decreasing functions of linear stiffness k . For case 2, the norm $\|\mathbf{U}\|$ for the second resonance peak remains the same while for the first resonance peak the norm $\|\mathbf{U}\|$ increases monotonically with the increase of uncertainty. Therefore, the quasi-periodic solutions obtained by the proposed method are in good excellent agreement with the MCS results. Hence, the proposed method is utilizable.

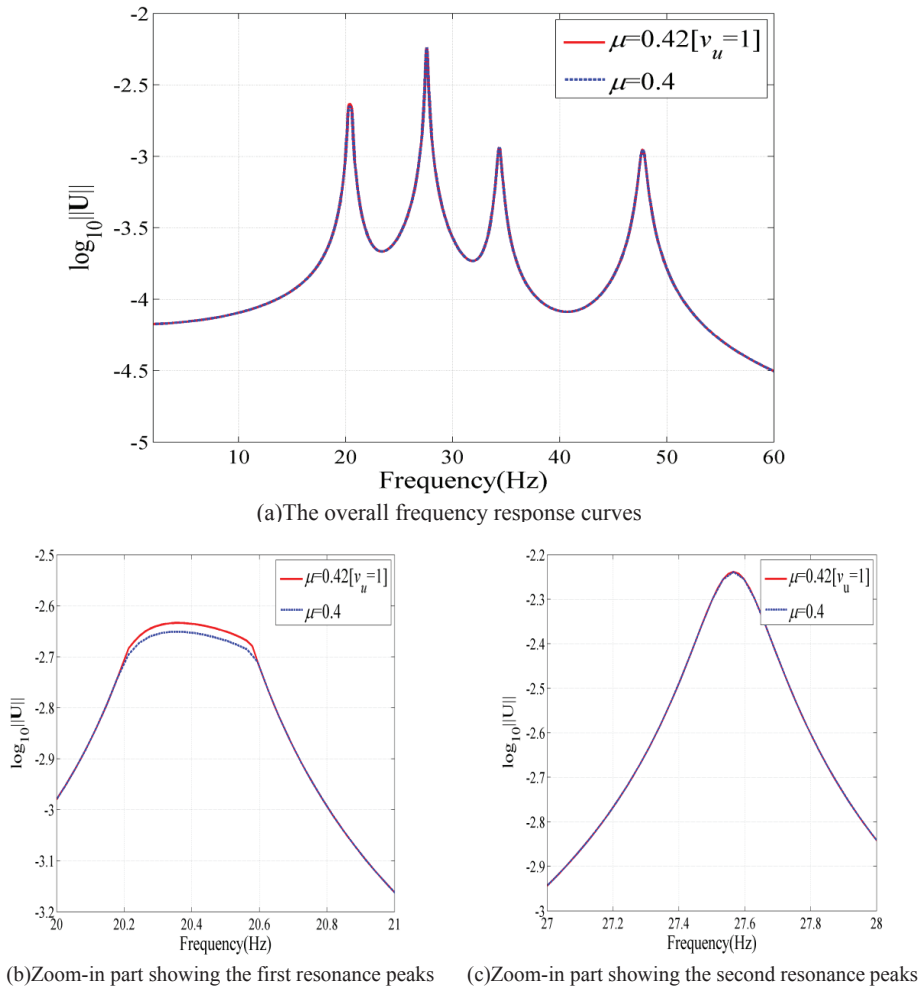


Figure 9: The frequency response curves for case 2

4 Conclusions

An efficient method is presented for finding the worst quasi-periodic vibration response of nonlinear dynamical systems. The proposed method which is based on the multi-dimensional harmonic balance method and the MultiStart optimization algorithm is formulated as a constrained, nonlinear optimization problem. By means of the multi-dimensional harmonic balance method, nonlinear differential equations are converted into a set of nonlinear algebraic equations. The multi-

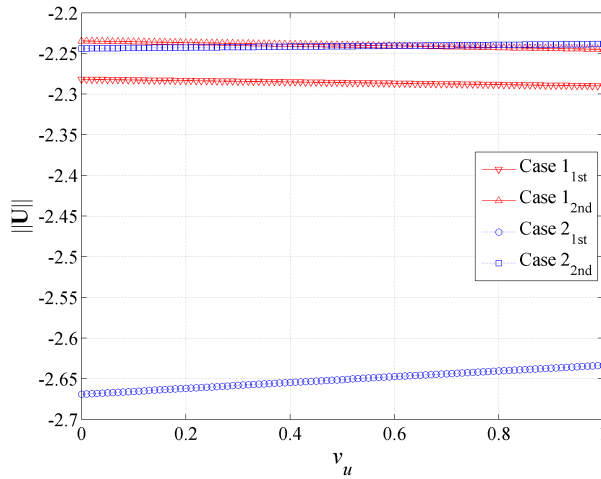


Figure 10: The Monte Carlo simulation results

dimensional harmonic balance nonlinear algebraic equations are then used to construct the general nonlinear equality constraints. Finally, the MultiStart algorithm is used to optimize the vibration response within the specified range of physical parameters.

In order to illustrate the efficiency and ability of the proposed method, two nonlinear dynamical systems are investigated: a canonical Duffing oscillator and a nonlinear two-degree-of-freedom model with different types of nonlinearities and uncertainties. Numerical examples show that the proposed approach is valid and effective for analyzing strongly nonlinear vibration problems with different types of nonlinearities in the presence of uncertainties.

Acknowledgement: The author is grateful to the anonymous referees for their valuable comments. This study has been financially supported by Natural Science Foundation of China (Project No.10904178).

References

- Alexander, N. A.** (2010): Estimating the nonlinear resonant frequency of a single pile in nonlinear soil. *J Sound Vib*, vol. 329, no. 8, pp. 1137-1153.
- Cameron, T. M.; Griffin, J. H.** (1989): An alternating frequency/time domain method for calculating the steady-state response of nonlinear dynamic systems. *J Appl Mech*, vol. 56, no. 1, pp. 149-154.

Chua, L.; Ushida, A. (1981): Algorithms for computing almost periodic steady-state response of nonlinear systems to multiple input frequencies. *Circ Syst*, vol. 28, no. 10, pp. 953-971.

Cochelin, B.; Vergez, C. (2009): A high order purely frequency-based harmonic balance formulation for continuation of periodic solutions. *J Sound Vib*, vol. 324, no. 1, pp. 243-262.

Dai, H. H.; Schnoor, M.; Atluri, S. N. (2012): A Simple collocation scheme for obtaining the periodic solutions of the Duffing equation, and its equivalence to the high dimensional harmonic balance method: subharmonic oscillations. *CMES: Computer Modeling in Engineering and Sciences*, vol. 84, pp. 459-498.

Dai, H. H.; Yue, X. K.; Yuan, J. P. (2013): A time domain collocation method for obtaining the third superharmonic solutions to the Duffing oscillator. *Nonlinear Dynamics*, vol. 73, no. 1-2, pp. 593-609.

Didier, J.; Sinou, J. J.; Faverjon, B. (2012): Study of the non-linear dynamic response of a rotor system with faults and uncertainties. *J Sound Vib*, vol. 331, pp. 671-703.

Didier, J.; Sinou, J. J.; Faverjon, B. (2013): Nonlinear vibrations of a mechanical system with non-regular nonlinearities and uncertainties. *Commun Nonlinear Sci Numer Simul*, vol.18, pp. 3250-3270.

Fletcher, R. (2013): *Practical methods of optimization*. John Wiley & Sons.

Guskov, M.; Sinou, J. J.; Thouverez, F. (2008): Multi-dimensional harmonic balance applied to rotor dynamics. *Mech Res Commun*, vol.35, no.8, pp. 537-545.

Guskov, M.; Thouverez, F. (2012): Harmonic balance-based approach for quasi-periodic motions and stability analysis. *J Vib Acoust*, vol. 134, no. 3, pp. 031003-1/11.

Hall, K. C.; Thomas, J. P.; Clark, W. S. (2002): Computation of unsteady non-linear flows in cascades using a harmonic balance technique. *AIAA J*, vol. 40, no. 5, pp. 879-886.

Jaumouillé, V.; Sinou, J. J.; Petitjean, B. (2010): An adaptive harmonic balance method for predicting the nonlinear dynamic responses of mechanical systems—Application to bolted structures. *J Sound Vib*, vol. 329, no. 19, pp. 4048-4067.

Kim, Y. B.; Choi, S. K. (1997): A multiple harmonic balance method for the internal resonant vibration of a non-linear Jeffcott rotor. *J Sound Vib*, vol. 208, no.5, pp. 745-761.

Kim, Y. B.; Noah, S. T. (1996): Quasi-periodic response and stability analysis for a non-linear Jeffcott rotor. *J Sound Vib*, vol. 190, no.2, pp. 239-253.

LaBryer, A.; Attar, P. J. (2009): High dimensional harmonic balance dealiasing

- techniques for a duffing oscillator. *J Sound Vib*, vol. 324, no. 3, pp. 1016-1038.
- Lau, S. L.; Cheung, Y. K.** (1981): Amplitude incremental variational principle for nonlinear vibration of elastic systems. *J Appl Mech*, vol. 48, pp. 959-964.
- Lau, S. L.; Cheung, Y. K.** (1983): Incremental harmonic balance method with multiple time scales for aperiodic vibration of nonlinear systems. *J Appl Mech*, vol. 50, no. 1, pp. 871-876.
- Laxalde, D.; Thouverez, F.; Sinou, J. J.** (2007): Qualitative analysis of forced response of blisks with friction ring dampers. *Eur J Mech A Solids*, vol. 26, no. 4, pp. 676-687.
- Liu, L.; Dowell, E. H.; Thomas, J. P.** (2007): A high dimensional harmonic balance approach for an aeroelastic airfoil with cubic restoring forces. *J Fluids Struct*, vol. 23, no. 3, pp. 351-363.
- Liu, L.; Thomas, J. P.; Dowell, E. H.** (2006): A comparison of classical and high dimensional harmonic balance approaches for a Duffing oscillator. *J Comput Phys*, vol. 215, no. 1, pp. 298-320.
- Millman, D. R.; King, P. I.; Beran, P. S.** (2005): Airfoil pitch-and-plunge bifurcation behavior with Fourier chaos expansions. *J Aircraft*, vol. 42, no. 2, pp. 376-384.
- Moens, D.; Vandepitte, D.** (2005): A survey of non-probabilistic uncertainty treatment in finite element analysis. *Comput Method Appl Mech Eng*, vol. 194, no. 12, pp. 1527-1555.
- Nacivet, S.; Pierre, C.; Thouverez, F.** (2003): A dynamic Lagrangian frequency-time method for the vibration of dry-friction-damped systems. *J Sound Vib*, vol. 265, no. 1, pp. 201-219.
- Nocedal, J.; Wright, S.** (2006): *Numerical optimization, series in operations research and financial engineering*. Springer.
- Pušenjāk, R. R.; Oblak, M. M.** (2004): Incremental harmonic balance method with multiple time variables for dynamical systems with cubic non-linearities. *Int J Num Meth Eng*, vol. 59, no. 2, pp. 255-292.
- Sarrouy, E.; Dessombz, O.; Sinou, J. J.** (2013): Stochastic study of a non-linear self-excited system with friction. *Eur J Mech A Solids*, vol. 40, pp. 1-10.
- Sarrouy, E.; Thouverez, F.** (2010): Global search of non-linear systems periodic solutions: A rotordynamics application. *Mech Syst Signal Process*, vol. 24, no. 6, pp. 1799-1813.
- Sinou, J. J.; Faverjon, B.** (2012): The vibration signature of chordal cracks in a rotor system including uncertainties. *J Sound Vib*, vol. 331, no. 1, pp. 138-154.

Ugray, Z.; Lasdon, L.; Plummer, J. (2007): Scatter search and local NLP solvers: A multistart framework for global optimization. *INFORMS Journal on Computing*, vol. 19, no. 3, pp. 328-340.

Wu, J.; Zhang, Y.; Chen, L. (2013): A Chebyshev interval method for nonlinear dynamic systems under uncertainty. *Appl Math Model*, vol. 37, no. 6, pp. 4578-4591.